Stem Cell Reports
Article

OPEN ACCESS

Neurite Aggregation and Calcium Dysfunction in iPSC-Derived Sensory Neurons with Parkinson's Disease-Related *LRRK2* G2019S Mutation

Andrew J. Schwab[1] and Allison D. Ebert[1,*]
[1]Department of Cell Biology, Neurobiology and Anatomy, Medical College of Wisconsin, 8701 Watertown Plank Road, Milwaukee, WI 53226, USA
*Correspondence: aebert@mcw.edu
http://dx.doi.org/10.1016/j.stemcr.2015.11.004

SUMMARY

Mutations in *leucine-rich repeat kinase 2* (*LRRK2*) are the most-common genetic determinants of Parkinson's disease (PD). The G2019S mutation is detected most frequently and is associated with increased kinase activity. Whereas G2019S mutant dopamine neurons exhibit neurite elongation deficits, the effect of G2019S on other neuronal subtypes is unknown. As PD patients also suffer from non-motor symptoms that may be unrelated to dopamine neuron loss, we used induced pluripotent stem cells (iPSCs) to assess morphological and functional properties of peripheral sensory neurons. *LRRK2* G2019S iPSC-derived sensory neurons exhibited normal neurite length but had large microtubule-containing neurite aggregations. Additionally, *LRRK2* G2019S iPSC-derived sensory neurons displayed altered calcium dynamics. Treatment with LRRK2 kinase inhibitors resulted in significant, but not complete, morphological and functional rescue. These data indicate a role for LRRK2 kinase activity in sensory neuron structure and function, which when disrupted, may lead to sensory neuron deficits in PD.

INTRODUCTION

Parkinson's disease (PD) is recognized by a variety of progressive motor symptoms, with the majority of PD patients also suffering from non-motor symptoms that can occur before motor symptoms appear and may be independent of dopamine neuron loss (Gaig et al., 2014; Pont-Sunyer et al., 2015; van der Heeden et al., 2014). Evidence of pathological changes in the dorsal root ganglia and the vagus, glossopharyngeal, and internal superior laryngeal peripheral nerves is rapidly accumulating (Mu et al., 2013a, 2013b). Lewy body pathology has also been observed in the dorsal vagus ganglion and parasympathetic nuclei, enteric nervous system, and cardiac and pelvic plexus (Wakabayashi and Takahashi, 1997; Orimo et al., 2008; Beach et al., 2010; Tysnes et al., 2010; Cersosimo and Benarroch, 2012). It remains to be determined whether peripheral neuron damage precipitates the development of non-motor symptoms in PD, but focused analysis on the peripheral nervous system may ultimately provide information leading to broad therapeutic intervention.

Most cases of PD are sporadic, but familial mutations account for nearly 10% of patients with PD (Toulouse and Sullivan, 2008). Mutations in *leucine-rich repeat kinase 2* (*LRRK2*) cause an autosomal dominant form of PD that is clinically indistinguishable from sporadic PD (Marras et al., 2011; Alcalay et al., 2013; Gatto et al., 2013; Trinh et al., 2014). LRRK2 is a multi-domain kinase that exists as a dimer under physiological conditions, and several studies have indicated that the G2019S mutation significantly increases kinase activity (West et al., 2005; Greggio et al., 2006; Jaleel et al., 2007; Luzón-Toro et al., 2007; Anand et al., 2009; Covy and Giasson, 2009). Although the underlying pathogenesis of PD remains poorly understood, increased LRRK2 kinase activity likely plays a key role in *LRRK2*-linked PD (Greggio et al., 2006; MacLeod et al., 2006; Smith et al., 2006; Lee et al., 2010; Deng et al., 2011).

The function of LRRK2 remains to be fully elucidated, but studies have demonstrated a role for LRRK2 in neurite elongation and arborization. Cultured dopaminergic neurons from human *LRRK2*-G2019S-expressing transgenic mice and patient-specific induced pluripotent stem cells (iPSCs) display shortened neurites and reduced neurite complexity (Ramonet et al., 2011; Cooper et al., 2012; Sánchez-Danés et al., 2012; Reinhardt et al., 2013). The molecular basis underlying the effects of LRRK2 on neurite growth and integrity is not known, though putative LRRK2 effectors have been implicated in the regulation of neurite outgrowth including ezrin, radixin, and moesin (ERM), which play roles in cytoskeletal dynamics. Increased LRRK2 activity has been correlated with increased ERM phosphorylation and decreased axon extension (Parisiadou et al., 2009).

Although sensory nerve disruption in PD has been reported by functional assessments of cutaneous sensory nerve endings and post-mortem analysis (Dabby et al., 2006; Ikemura et al., 2008; Nolano et al., 2008; Shishido et al., 2010; Toth et al., 2010), there are limited data on the effect of LRRK2 on sensory neuron structure and function. We sought to investigate whether PD mutations confer intrinsic defects in sensory neuron structure and function using iPSCs. We compared sensory neurons derived from two PD patients with homozygous *LRRK2* G2019S mutations and one asymptomatic patient

Table 1. Description of the Different Control and PD Cell Lines Used

Line	Mutation	Sex	Age of Sampling	Age of Onset	Method of Reprogramming	Source
GM03814 (control 1)	N/A	F	unknown	NA	lentiviral	purchased fibroblasts from Coriell; iPSC generation described in Ebert et al., 2009
GM02183 (control 2)	N/A	F	21	NA	Sendai	purchased fibroblasts from Coriell; iPSC generation in house
K3 (control 3)	N/A	M	newborn	NA	transient transfection of plasmid DNA encoding reprogramming factors	iPSCs obtained from Dr. Stephen Duncan, described in Si-Tayeb et al., 2010
ND34391*E (SNCA 3×)	SNCA triplication	F	55	50	retroviral	purchased iPSC line from Coriell
ND40019*C (LRRK2 G2019S het)	G2019S heterozygous	M	unknown	NA	retroviral	purchased iPSC line from Coriell
ND35367*C (LRRK2 G2019S 1)	G2019S homozygous	M	79	50	retroviral	purchased iPSC line from Coriell
ND40018*C (LRRK2 G2019S 2)	G2019S homozygous	F	60	48	retroviral	purchased iPSC line from Coriell

heterozygous for *LRRK2* G2019S to one PD patient with *α-synuclein* (*SNCA*) triplication and three unaffected individuals. Dopamine neurons derived from the mutant *LRRK2* lines showed shortened neurites and reduced neurite branching, consistent with other well-characterized models of *LRRK2* PD. In contrast, *LRRK2* G2019S iPSC-derived sensory neurons exhibited normal neurite outgrowth but increased cytoskeletal aggregations and altered calcium dynamics compared to control or *SNCA* iPSC-derived sensory neurons. Treatment with LRRK2 kinase inhibitors resulted in significant but incomplete morphological and functional rescue. Together, these data indicate that excessive LRRK2 kinase activity can negatively impact sensory neuron structure and function and may play a role in the development of sensory dysfunction in PD.

RESULTS

Sensory Differentiation and Characterization from PD and Control iPSCs

To examine the functional properties of PD sensory neurons, we utilized human iPSCs derived from multiple PD patients (Table 1). We cultured iPSCs from an *α-synuclein* triplication line (referred to as *SNCA* (3×)), two homozygous *LRRK2* G2019S lines (referred to as *LRRK2* G2019S 1 and 2), a heterozygous *LRRK2* G2019S line (referred to as *LRRK2* G2019S het), and three unaffected control lines (referred to as control 1, 2, and 3). The iPSCs were grown as adherent monolayers and then differentiated into peripherin-positive peripheral sensory neurons using a previously established protocol (Chambers et al., 2012). Generation of peripherin- and βIII-tubulin-positive neurons was assessed by immunocytochemistry at 4 and 6 weeks of differentiation (Figure 1A). Importantly, all PD and control iPSCs generated equivalent numbers of peripheral sensory neurons based on the expression of βIII tubulin (30%–40%) and peripherin (~20%; Figures 1B and 1C) with similar neurite lengths (Figure 1D). Additional immunocytochemical and functional characterization of the sensory neuron subtype of TrkA- and TRPV1-expressing nociceptors showed differentiation efficiency was equivalent across all iPSC lines (Figure S1).

Neurite Outgrowth Abnormalities and Aggregate Formation in *LRRK2* G2019S iPSCs

Despite the fact that all PD iPSC lines tested generated similar numbers of peripheral sensory neurons, *LRRK2* G2019S iPSCs exhibited specific neurite deficits. *LRRK2* G2019S iPSC-derived sensory neurons displayed significantly more and larger neurite aggregates compared to control and *SNCA* (3×) iPSC-derived sensory neurons (Figures 2A–2C). Neurite aggregates have been observed in many different neurodegenerative diseases including PD (MacLeod et al., 2006) and may be an indicator of early stages of axonopathy. Neurite aggregates may be a prominent feature of the *LRRK2* G2019S mutation as the phenotype was not observed in *SNCA* (3×) iPSC-derived sensory neurons (Figure 2B) and was also absent from peripheral sensory neurons derived from other diseased iPSCs (Schwab and Ebert, 2014). Immunocytochemistry for ATF3, a transcription factor activated in sensory neurons following nerve injury (Tsujino et al., 2000; Lindå

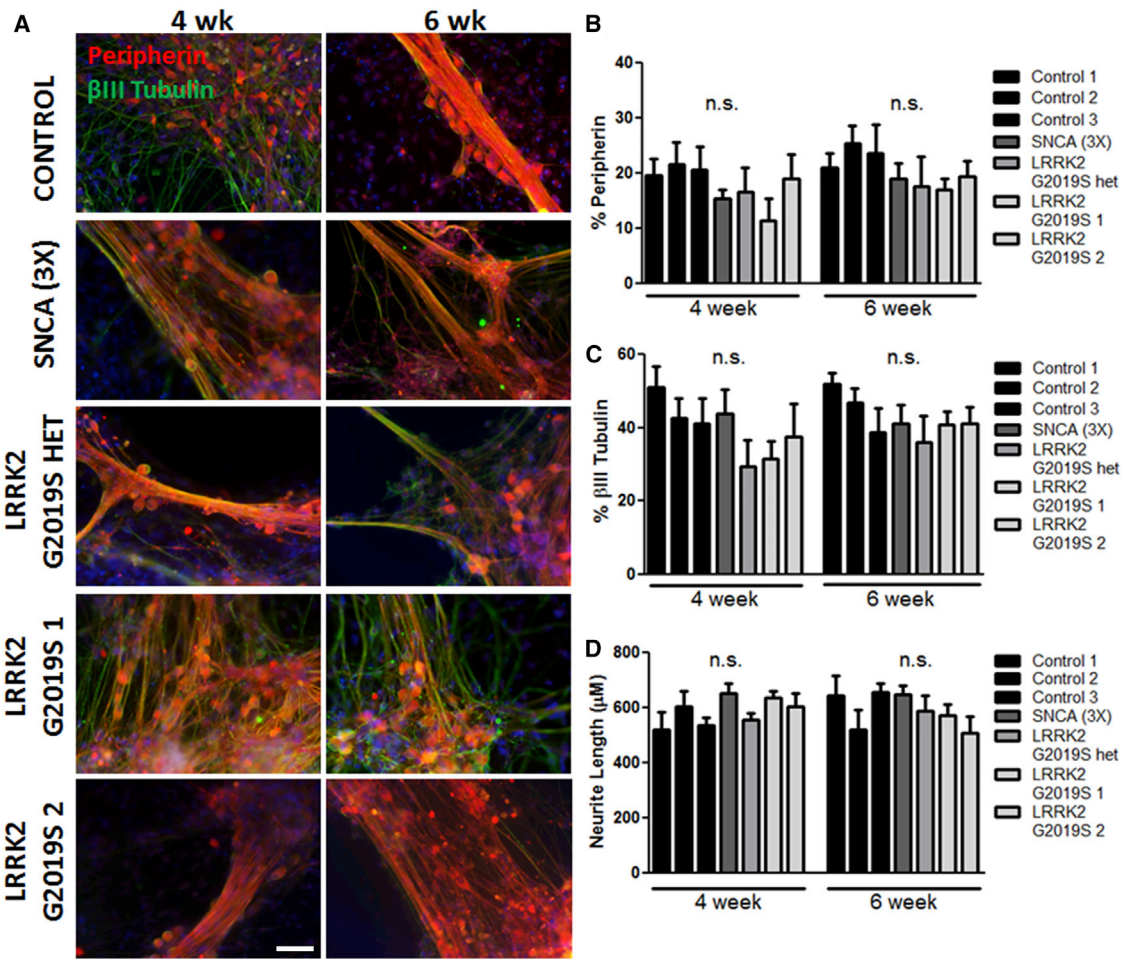

Figure 1. Peripherin-Positive Sensory Neurons at 4 and 6 Weeks of Differentiation

(A) Control and PD iPSCs acquired a βIII tubulin+ (green)/peripherin+ (red) sensory neuron phenotype. Nuclei are labeled with Hoechst (blue).

(B and C) Quantification of peripherin+ (B) and βIII tubulin+ (C) sensory neurons showed no significant difference in neuronal differentiation efficiency between control and PD iPSCs.

(D) There was no difference in neurite length between control and PD iPSC-derived sensory neurons.

n.s., not significant by one-way ANOVA at each time point; n = 6 independent experiments. The scale bar represents 50 μm. See also Figure S1.

et al., 2011), was not increased in *LRRK2* G2019S cultures (data not shown), indicating minimal peripheral nerve damage.

The sensory neuron data are in contrast to the phenotype observed in *LRRK2* G2019S iPSC-derived dopamine neurons. Similar to previous studies (Cooper et al., 2012; Sánchez-Danés et al., 2012; Reinhardt et al., 2013), we found that *LRRK2* G2019S iPSC-derived dopamine neurons exhibited significantly shortened neurites and reduced neurite arborization but no increase in neurite aggregation compared to controls (Figures S2A–S2D). We hypothesized that neurite length was too short to induce significant aggregate formation in *LRRK2* G2019S iPSC-derived dopamine neurons. To test this, we cultured *LRRK2* G2019S iPSC-derived dopamine neurons with nerve growth factor (NGF), a potent growth factor for neurite outgrowth used in the sensory neuron differentiation medium. NGF treatment significantly restored neurite length to control levels compared to untreated *LRRK2* G2019S dopamine neurons (Figure S2E), but aggregate numbers were unchanged (data not shown). Similarly, treatment with the LRRK2 kinase inhibitor LRRK2-IN-1 also restored neurite length without the development of neurite aggregates (data not shown). We next considered that levels of phosphorylated and total LRRK2 may differentially affect dopamine and sensory neurons; however, we found no significant

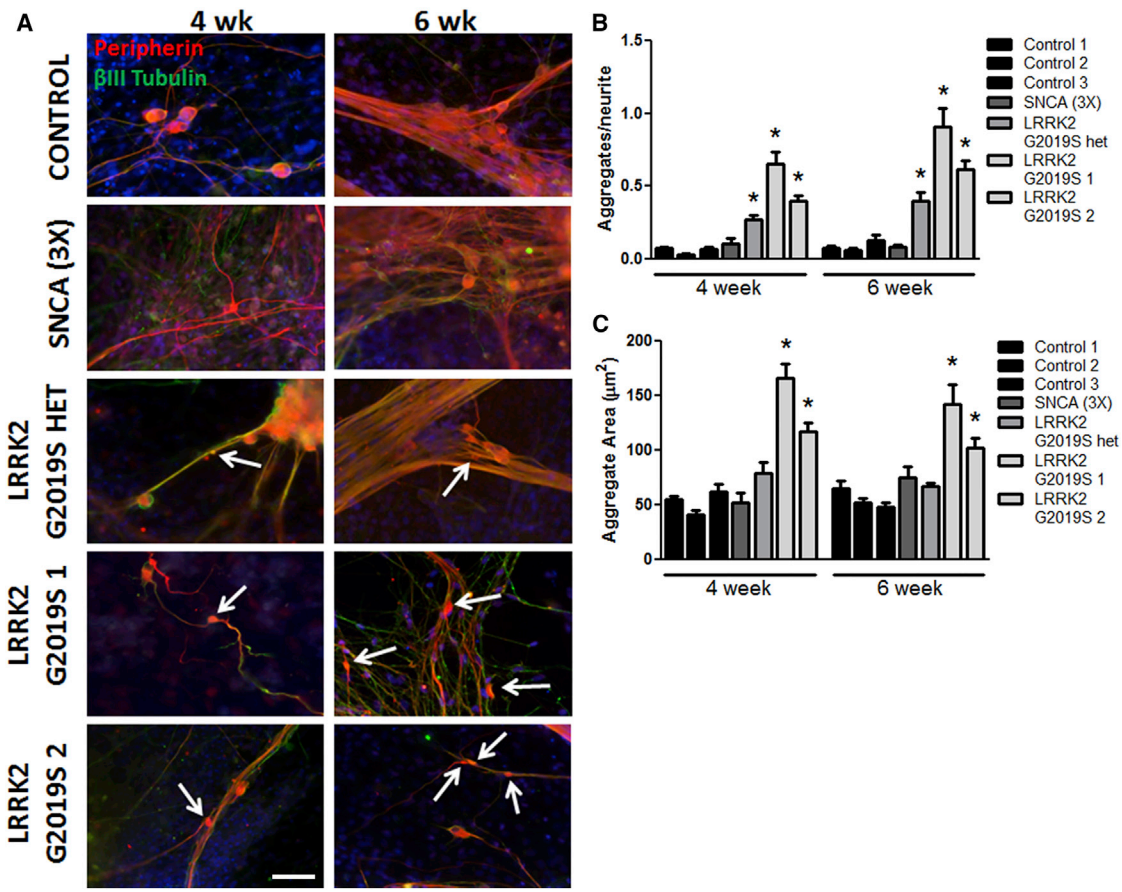

Figure 2. *LRRK2* G2019S iPSC-Derived Sensory Neurons Display Neurite Aggregate Formation

(A) *LRRK2* G2019S sensory neurons showed abnormal neurite patterns and increased aggregates along the neurites (white arrows).

(B) The number of aggregates per neurite was significantly increased in *LRRK2* G2019S neurons compared to all other groups by one-way ANOVA within each time point.

(C) The aggregate area was significantly increased in both *LRRK2* G2019S 1 and 2 compared to all other groups by Kruskal-Wallis test.

*$p < 0.01$; n = 4 independent experiments. The scale bar represents 50 μm. See also Figure S2.

differences in protein expression between the two neuron subtypes (Figure S2F). These data indicate that *LRRK2* G2019S alters cytoskeletal structure but that defects manifest differently in sensory neurons and dopamine neurons.

We next sought to determine the composition of the neurite aggregates. Aggregates showed positive staining for peripherin and βIII tubulin, which are intermediate filament and microtubule proteins, respectively (Figure 3A). A proportion of aggregates were positive for the microtubule-associated protein tau (Figure 3A), although we did not observe tau phosphorylation by immunocytochemistry (data not shown). However, by western blot, we do observe an overall increase in tau and phosphorylated tau levels in *LRRK2* G2019S sensory neuron cultures compared to control and *SNCA* (3×) (Figures 3B–3D). Neurite aggregates were also positive for microtubule-associated protein 2 (MAP2) (Figure 3A). We found that some aggregates expressed LRRK2 (Figure 3A), but we did not observe LRRK2 phosphorylation by immunocytochemistry (data not shown). Overall expression of SNCA was low but highly variable from neuron to neuron as shown by immunocytochemistry (Figure S3A) and within the whole culture as shown by western blot (Figure S3B). As expected, the *SNCA* (3×) iPSC line had a global increase in SNCA expression compared to controls (Figures S3A–S3C) consistent with a gene triplication mutation. SNCA was increased in one *LRRK2* G2019S iPSC line, but not the others (Figures S3B and S3C), suggesting that SNCA levels do not accurately predict the development of aggregates in this system. At the aggregate level, some aggregates did express SNCA (Figure S3A), but the majority did not (Figure 3A). Finally, ubiquitin expression was not observed in the neurite aggregates (Figure 3A). Taken together, these results suggest that aggregates

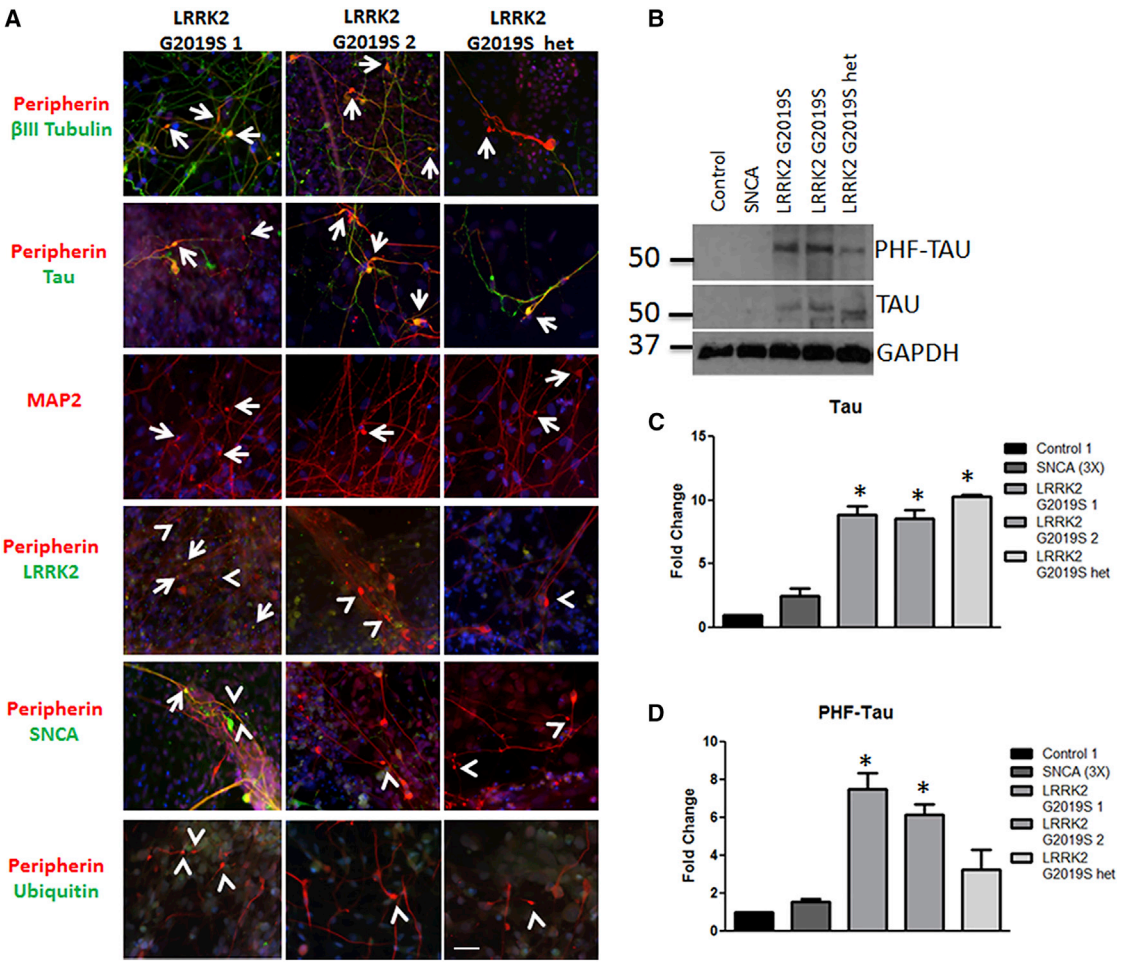

Figure 3. Aggregates Are Comprised of Cytoskeletal Proteins

(A) *LRRK2* G2019S aggregates were positive (indicated by arrows) for βIII tubulin (green) and peripherin (red), tau (green), MAP2 (red), and LRRK2 (green). Aggregates were generally negative (indicated by arrowheads) for SNCA and ubiquitin (green).

(B–D) *LRRK2* G2019S sensory neuron cultures display significantly increased levels of (B and C) tau and (B and D) phospho-tau by western blot and densitometry. *$p < 0.01$ by ANOVA; $n = 6$ independent experiments.

The scale bar represents 50 μm. See also Figure S3.

contain axonal and dendritic microtubule proteins and are likely distinct from classical Lewy bodies and Lewy neurites.

Altered Calcium Dynamics in *LRRK2* G2019S iPSC-Derived Sensory Neurons

Compared to control and *SNCA* (3×), sensory neurons with *LRRK2* G2019S mutations showed decreased calcium-mediated response to depolarization with 50 mM KCl (Figure 4). Sensory neurons derived from each of the *LRRK2* G2019S iPSC lines showed significant differences in this response compared to all controls and *SNCA* (3×) (Figures 4A–4C). Next, we investigated whether impaired calcium signaling affected autophagy as has been reported previously (Gómez-Suaga et al., 2012). We found a significant increase in p62 and LC3-II protein levels in *LRRK2* G2019S iPSC-derived sensory neurons compared to control and *SNCA* (3×) (Figures S4A–S4C). Collectively, these data suggest that the G2019S mutation compromises the ability of the iPSC-derived sensory neurons to efficiently respond to calcium signaling.

Pharmacological Inhibition of LRRK2 Kinase Activity Partially Rescues Morphological Abnormalities

To assess whether hyper-kinase activity was contributing to morphological abnormalities in *LRRK2* G2019S iPSC-derived sensory neurons, we treated sensory neurons with three different LRRK2 kinase inhibitors: LRRK2-IN-1; GSK2578215A; and CZC25146. Studies have shown LRRK2 is phosphorylated at Ser935 (Dzamko et al.,

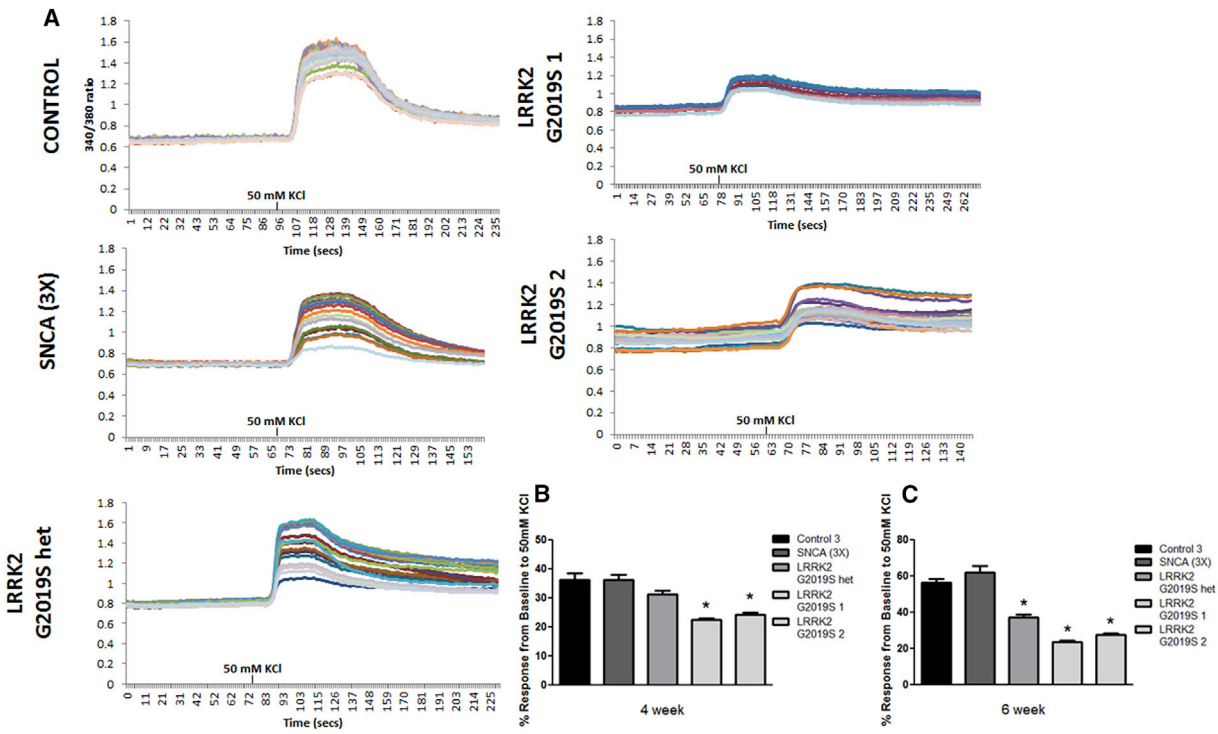

Figure 4. *LRRK2* G2019S and *LRRK2* G2019S het iPSC-Derived Sensory Neurons Display Abnormal Calcium Dynamics

(A) Representative calcium imaging traces of at least ten individual sensory neurons are shown for each line at 4 weeks of differentiation. KCl indicates the time at which the depolarizing stimulus was added to the cultures.

(B and C) Sensory neurons from each of the *LRRK2* G2019S iPSC lines displayed a significantly reduced response to KCl-induced depolarization at 4 and 6 weeks of differentiation compared to controls and *SNCA* (3×). *$p < 0.01$ by ANOVA to the controls and Student's t test to SNCA (3×); n = 6 independent experiments, totaling ≥100 neurons from each iPSC line.

See also Figure S4.

2010; Deng et al., 2011; Reith et al., 2012). Using western blot analysis, we observed that untreated *LRRK2* G2019S sensory neurons showed increased phosphorylation at Ser935 compared to control; as an indication of the effectiveness of kinase inhibition, western blot analysis indicated that all three kinase inhibitors reduced Ser935 phosphorylation without substantial alterations in total LRRK2 levels (Figure 5A). Kinase inhibition did not affect cell survival or differentiation (Figures 5B and 5C), but it did result in a significant decrease in neurite aggregation and reduced aggregate size compared to the untreated *LRRK2* G2019S condition (Figures 5D and 5E). LRRK2-IN-1 treatment did lead to increased aggregate formation, and all three inhibitors increased aggregate size in control sensory neurons. This negative effect on the control neurons may be due to possible off-target effects of LRRK2 kinase inhibition (Luerman et al., 2014). Additionally, not all inhibitors were equally effective (Figures 5D and 5E). Nevertheless, these results suggest that excessive LRRK2 kinase activity contributes to neurite aggregate formation.

Pharmacological Inhibition of LRRK2 Kinase Activity Improves Calcium Dynamics

To assess whether hyper-kinase activity was also contributing to diminished KCl-mediated calcium responses in *LRRK2* G2019S iPSC-derived sensory neurons, we treated sensory neuron cultures with LRRK2-IN-1, GSK2578215A, and CZC25146 kinase inhibitors for 2 weeks starting at 2 weeks of differentiation (Figure 6A). Live-cell calcium imaging analysis of sensory neurons treated with LRRK2 kinase inhibitors showed a significant increase in KCl-induced calcium response in *LRRK2* G2019S sensory neuron cultures; however, all treated groups were still significantly reduced compared to untreated control levels (Figures 6A and 6B). However, only treatment with GSK2578215A significantly improved calcium response to KCl depolarization in *LRRK2* G2019S het sensory neurons, which may be indicative of greater LRRK2 specificity (Reith et al., 2012). In contrast, control sensory neurons exhibited a decreased calcium response to KCl after CZC25146 treatment, which may be attributed to off-target effects. We tested whether lower dosages of GSK2578215A

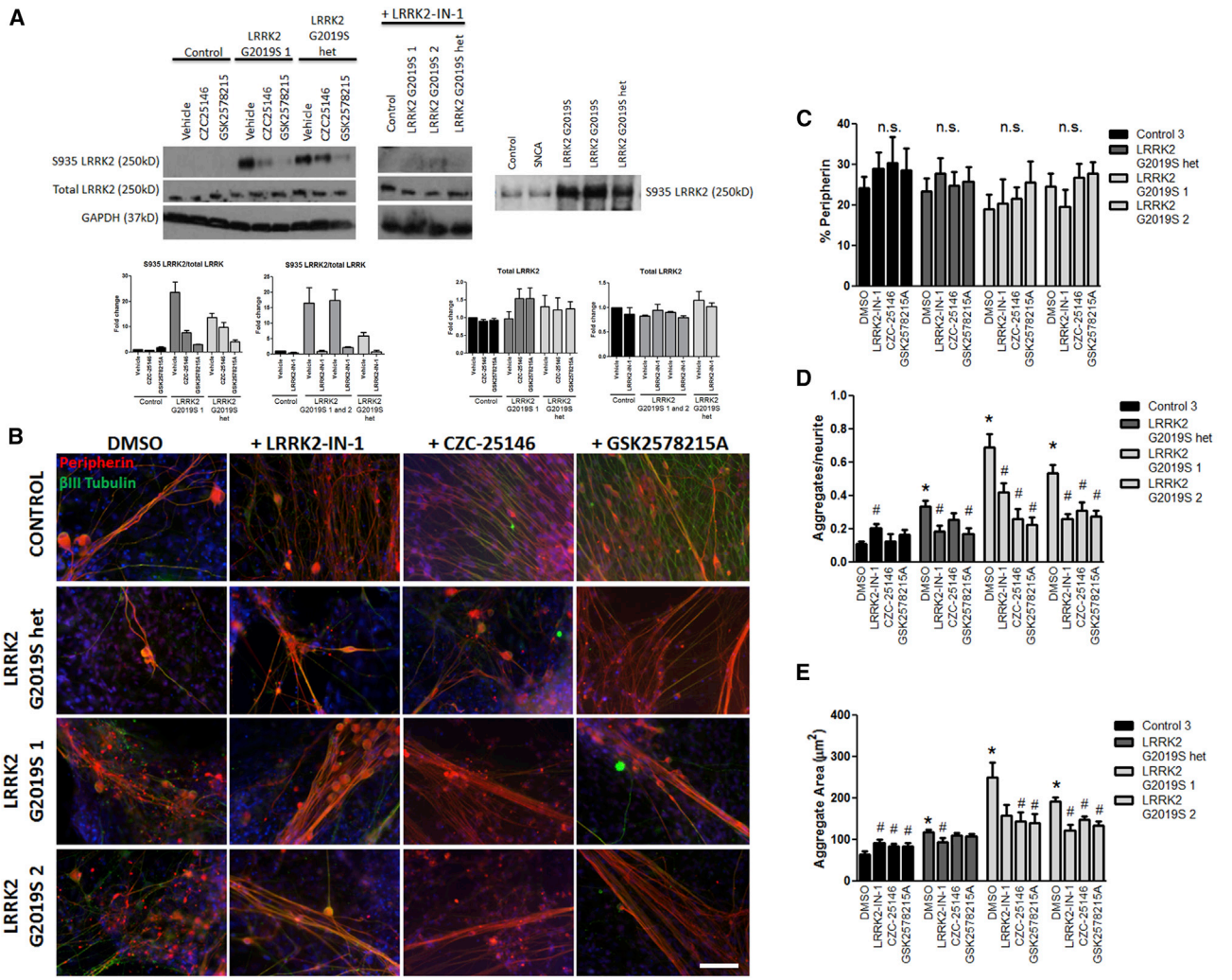

Figure 5. Pharmacologically Inhibiting LRRK2 Kinase Activity Partially Rescues Morphological Abnormalities

(A) LRRK2-IN-1, CZC25146, and GSK2578215A treatment reduced phosphorylation of S935 in *LRRK2* G2019S sensory neurons as shown by western blot and densitometry. GAPDH was used as a protein loading control. For reference, longer exposure times allowed for the detection of S935 in control and *SNCA* (3×) samples.

(B and C) Representative peripherin (red) and βIII tubulin (green) images are shown for untreated and inhibitor treated conditions, with no significant impact on sensory neuron development or survival by one-way ANOVA. Nuclei are labeled in blue.

(D) LRRK2-IN-1, CZC25146, and GSK2578215A treatment significantly reduced the number of aggregates in sensory neurons derived from *LRRK2* G2019S 1 and 2 compared to their respective untreated condition by one-way ANOVA. LRRK2-IN-1 and GSK2578215A treatment reduced neurite aggregation in *LRRK2* G2019S het compared to its untreated condition by one-way ANOVA. CZC25146 treatment induced significant aggregate formation in control cells compared to its untreated condition by one-way ANOVA.

(E) LRRK2-IN-1, CZC25146, and GSK2578215A treatment of *LRRK2* G2019S 2 resulted in a significant decrease in neurite aggregate area, whereas only CZC25146 and GSK2578215A significantly rescued neurite aggregate area in *LRRK2* G2019S 1. Only LRRK2-IN-1 significantly decreased aggregate area in *LRRK2* G2019S het. All three inhibitors increased aggregate area in control cells by Kruskal-Wallis test.

n.s., not significant within each cell line. *$p < 0.01$ compared to untreated control and #$p < 0.01$ comparing treatment to the respective untreated condition. The scale bar represents 50 μm. n = 3 independent experiments totaling ≥50 neurons for each iPSC line.

(0.1 and 0.5 μM) for shorter durations would still be effective. An acute 1-day treatment was not sufficient to alter calcium responses to depolarization (data not shown). Lower doses were mostly ineffective, but a 1-week treatment with 1 μM was sufficient to significantly improve calcium responses to depolarization (Figure S5). Higher doses were not tested in an effort to avoid exacerbating any negative effects in control cells (e.g., Figures 5E and 6B). Interestingly,

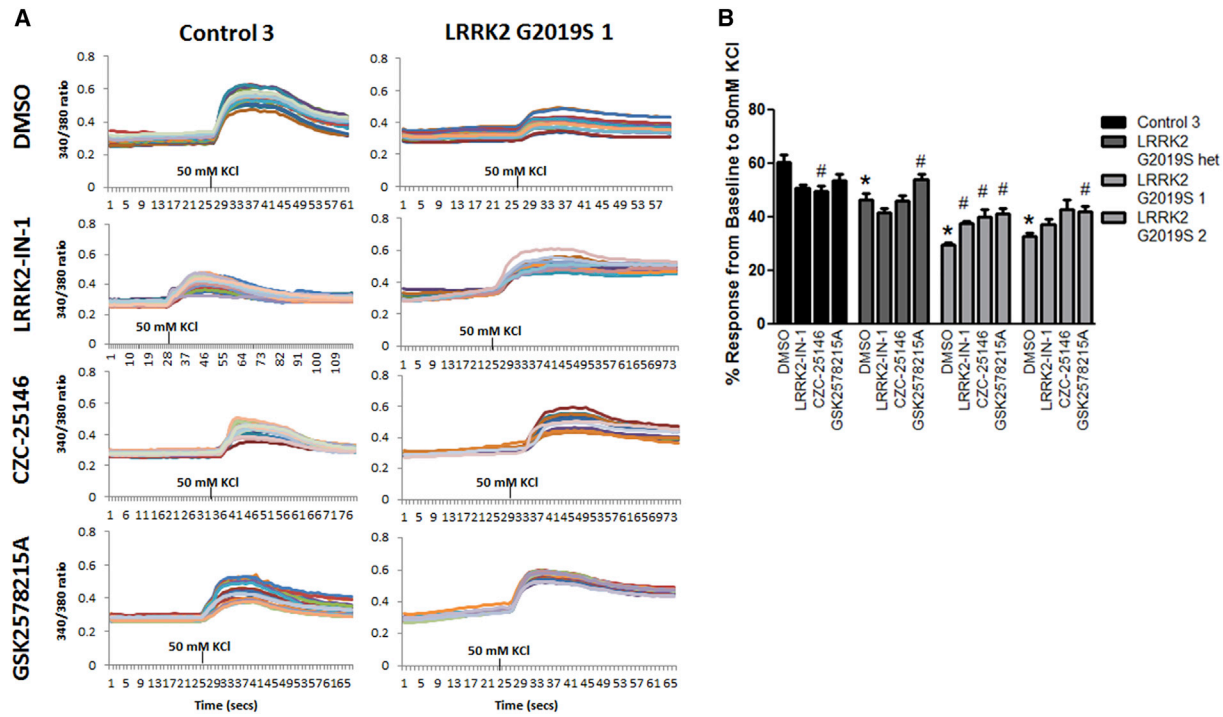

Figure 6. Pharmacologically Inhibiting LRRK2 Kinase Activity Partially Rescues Calcium Signaling Deficits

(A) Representative traces of at least ten sensory neurons are shown for control 3 and *LRRK2* G2019S 1 untreated and kinase-inhibitor-treated conditions at 4 weeks of differentiation.

(B) LRRK2-IN-1, CZC25146, and GSK2578215A treatment significantly increased calcium response to KCl in *LRRK2* G2019S 1 sensory neurons. Only GSK2578215A treatment significantly increased calcium response to KCl in *LRRK2* G2019S 2 and het sensory neurons. Control sensory neurons treated with CZC25146 resulted in a significantly decreased calcium response to KCl. *$p < 0.01$ compared to untreated control and #$p < 0.01$ comparing treatment to the respective untreated condition by Kruskal-Wallis test. $n = 3$ independent experiments totaling $\geq$100 neurons for each iPSC line.

See also Figure S5.

the autophagy markers p62 and LC3-II were unaffected by kinase inhibition (Figures S4A–S4C). These results suggest that increased kinase activity due to the G2019S mutation partially contributes to calcium-related defects in *LRRK2* G2019S iPSC-derived sensory neurons.

DISCUSSION

PD patients suffer from both motor and non-motor symptoms, and due to the differentiation capacity of iPSCs, we can take advantage of this system to study multiple cell types that may be impacted by disease processes. Consistent with other reports (Cooper et al., 2012; Sánchez-Danés et al., 2012; Reinhardt et al., 2013), we show that *LRRK2* G2019S iPSC-derived dopamine neurons display shortened neurites and reduced branching compared to controls. However, the same *LRRK2* G2019S mutation creates a different phenotype in peripheral sensory neurons. Specifically, we find neurite length is comparable to control cells, but the neurites harbor large cytoskeletal aggregates. Reinhardt and colleagues (2013) had previously found that Brn3a-positive sensory neurons derived from heterozygous *LRRK2* G2019S iPSCs did not exhibit increased cell death following treatment with rotenone, but no other aspects of sensory neuron structure or function have previously been studied. Although very little is known about the cause of somatosensory symptoms in PD, the observation of neurite aggregates within sensory neurons aligns with PD patients exhibiting peripheral nervous system impairment and may be a pathological feature of PD (Nolano et al., 2008; Donadio et al., 2014; Doppler et al., 2014). Additionally, intermediate filament- and peripherin-containing aggregates are commonly found in the peripheral axon of motor neurons in amyotrophic lateral sclerosis (Xiao et al., 2006), suggesting peripheral neurons and central neurons with peripheral targets may undergo common alterations in neurodegenerative diseases.

Using immunocytochemical analysis, we found that *LRRK2* G2019S iPSC-derived sensory neurons displayed

neurite aggregations comprised of PD-associated proteins β-tubulin, MAP2, Tau, LRRK2, and SNCA. β-tubulin, a component of Lewy bodies, has been shown to directly interact with LRRK2, which regulates tubulin phosphorylation and acetylation (Law et al., 2014). Moreover, tubulin interacts with a number of other PD-related proteins including SNCA, parkin, and tau (Alim et al., 2002; Yang et al., 2005; Gillardon, 2009; Kawakami et al., 2012; Law et al., 2014), which likely implicates microtubule dysfunction as a common mechanism leading to the clinical and pathological hallmarks of PD (Cartelli et al., 2012). Consistent with this, MAP2-positive neurite aggregates have been identified in dopaminergic and non-dopaminergic neurons in post-mortem PD brain (D'Andrea et al., 2001). Tau has been implicated in the pathogenesis of PD in recent genome-wide screens (Simón-Sánchez et al., 2009; Edwards et al., 2010) and is seen in animal models expressing *LRRK2* mutations (Li et al., 2009b; Lin et al., 2010; Melrose et al., 2010). LRRK2 has been shown to facilitate tau phosphorylation in a kinase-independent manner (Shanley et al., 2015), and our tau data align with previously reported data in *LRRK2* G2019S and I2020T iPSC-derived neurons (Reinhardt et al., 2013; Ohta et al., 2015). Tau hyperphosphorylation has been shown to favor tau detachment from microtubules (Lindwall and Cole, 1984) that can lead to neurofibrillary tangle formation. Moreover, in a *hLRRK2* (R1441G) BAC transgenic mouse model, fragmented axons, axonal spheroids, and dystrophic neurites were observed and found to be associated with abnormally phosphorylated tau (Li et al., 2009a). Together with our data, these observations suggest a role of LRRK2 in tau-related neuronal pathology, which may be contributing to the increased neurite aggregate formation in iPSC-derived sensory neurons.

The contribution of LRRK2 to PD pathology has yet to be fully elucidated. LRRK2 has been proposed to act upstream of SNCA and tau to promote aggregation, but it may also act independently to promote neuron loss in the absence of aggregate pathology (Taymans and Cookson, 2010). Additionally, in some experimental cell culture systems, *LRRK2* G2019S mutation has been shown to generate numerous protein aggregates (Greggio et al., 2006), whereas in others it does not (Kett et al., 2012). Together, these data indicate a need for better understanding of cell-type-specific LRRK2 functions. Our data also suggest that the aggregates are distinct from traditional Lewy bodies and form independent of SNCA expression levels. The lack of aggregate formation in *SNCA* (3×) iPSC sensory neurons may be further indication of divergent LRRK2 and SNCA pathways leading to cellular dysfunction in PD. The low level of SNCA-positive aggregations in the *LRRK2* iPSCs is somewhat surprising as many LRRK2 cases show SNCA Lewy body pathology (Giasson and Van Deerlin, 2008; Hasegawa et al., 2009). However, some *LRRK2* PD patients do not develop Lewy body pathology (Cookson et al., 2008), and a number of experimental models of *LRRK2*-associated PD exhibit protein aggregations and/or inclusions that do not associate with SNCA (Waxman et al., 2009; Tsika et al., 2015). Differences in experimental models, such as species, neuron subtype, LRRK2 expression levels, and antibody epitopes and/or specificity may contribute to variations in results (Zhu et al., 2006; Melrose et al., 2007). Nevertheless, these data all indicate mutant LRRK2 can disrupt neurite integrity in multiple neuronal systems and may promote neuron dysfunction and death. Specifically, how LRRK2 is affecting microtubule stability in sensory neurons needs further investigation, but the robust aggregate phenotype found in *LRRK2* G2019S iPSC neurons will be a valuable system to address this.

Using live-cell calcium imaging analysis, we found that *LRRK2* G2019S iPSC-derived sensory neurons display diminished calcium responses to KCl depolarization. As calcium is critical for proper neuronal signaling and function, any perturbation could be detrimental. Dysregulated calcium is evident in mutant *LRRK2* neurons. For example, others showed that mutant *LRRK2*-expressing mouse cortical neurons had reduced calcium recovery and efflux (Cherra et al., 2013). Altered calcium levels can lead to aberrations in lysosomal clearance, followed by an increase in proteostatic stress. In this regard, Gómez-Suaga et al. (2012) showed that overexpression of wild-type or G2019S LRRK2 caused an increase in autophagosomes through calcium-dependent activation of the CaMKK/AMPK pathway, which could be inhibited by calcium chelation. Autophagosome accumulation in the *LRRK2* G2019S iPSC-derived sensory neurons further indicates impairment of the autophagy-lysosome system in LRRK2-mediated PD. However, the neuron-subtype-specific consequences of calcium dysregulation and subsequent altered autophagy signaling remain to be determined in relation to pathological mechanisms in PD.

Finally, our findings further support the idea that kinase activity is playing a role in *LRRK2*-G2019S-induced neuronal dysfunction. Inhibition of LRRK2 kinase activity using LRRK2-IN-1, GSK2578215A, or CZC25146 resulted in partial but significant functional and morphological rescue in homozygous and heterozygous *LRRK2* G2019S iPSC-derived sensory neurons. Individual kinase inhibitors show differing efficacy in the parameters tested, but treatment with GSK2578215A most consistently resulted in significant aggregate reduction and calcium signaling improvement in both the homozygous and heterozygous contexts. However, neither outcome measure was rescued to control levels, nor were levels of autophagosome markers improved. This could be due to suboptimal inhibitor dosages or treatment paradigms, but it is also possible

that other functional domains of LRRK2 contribute to sensory neuron dysfunction. For example, mutations in the GTPase domain result in neurite aggregations in transgenic mice (Li et al., 2009b). GTPase activity has been shown to modulate kinase activity, and it has been proposed that the GTPase and kinase domains may reciprocally regulate each other to direct the function of LRRK2 (Biosa et al., 2013), thereby necessitating further consideration of the potential pathogenic interplay between LRRK2 functional domains.

Disease modeling with iPSCs can be challenging due to inherent patient variability and line-to-line differences (Hu et al., 2010; Boulting et al., 2011). Importantly, very few differences were observed among the three independent control lines. The *SNCA* (3×) iPSC line was not different from controls in the parameters tested, but one *SNCA* (3×) line is not sufficient to conclude this line does not exhibit other PD-related phenotypes. The two homozygous *LRRK2* G2019S iPSC lines used here showed slight variation in the extent of the dysfunction, with *LRRK2* G2019S 1 generally being more affected. However, both lines were consistently impaired relative to control cells and the *SNCA* (3×) line. The heterozygous *LRRK2* G2019S iPSC-derived sensory neurons exhibited a less-severe phenotype than sensory neurons derived from either homozygous *LRRK2* G2019S iPSC line. This could be due to the fact that the heterozygous *LRRK2* G2019S iPSC line was generated from an asymptomatic patient. Alternatively, it could be due to a dosage effect of mutant LRRK2. Nevertheless, the heterozygous mutant *LRRK2* iPSC-derived neurons did exhibit significant structural and functional abnormalities consistent with the dominant nature of *LRRK2* mutations. Despite minor variations among the three *LRRK2* G2019S iPSC lines, our data report a robust aggregate and calcium phenotype in *LRRK2* G2019S iPSC-derived sensory neurons that provides the foundation for additional optimization and evaluation across a larger cohort of *LRRK2* patient samples. The iPSC-based model of PD offers a valuable tool to study the pathophysiology of LRRK2-related defects in multiple cell types affected in PD and may provide a mechanistic link between cytoskeletal changes, neuron dysfunction, and the appearance of motor and non-motor symptoms in PD.

EXPERIMENTAL PROCEDURES

Cell Culture

Human iPSCs were obtained from commercially available samples of an *SNCA* triplication line (ND34391*E; Coriell Institute), two *LRRK2* G2019S lines (ND35367*C and ND40018*C; Coriell Institute), and a heterozygous *LRRK2* G2019S line (ND40019*C; Coriell Institute). Three previously characterized unaffected control lines were used (GM003814 Coriell Institute, GM02183 Coriell Institute, and iPSK3; Ebert et al., 2009; Si-Tayeb et al., 2010; HD iPSC Consortium, 2012). iPSCs were grown in feeder-free conditions on Matrigel substrate in Nutristem medium (Stemgent) and used between passages 5 and 15. Neural progenitor cells (EZ Spheres) were generated and maintained as previously described (Ebert et al., 2013). The use of iPSCs was approved by the Medical College of Wisconsin's Human Stem Cell Research Oversight Committee.

Neural Differentiation

EZ spheres were differentiated into dopamine neurons using FGF-8, purmorphamine, and growth factors as previously described (Ebert et al., 2013). Induction of sensory neurons was accomplished using an established protocol (Chambers et al., 2012). For kinase inhibition experiments, 1 μM LRRK2-IN-1, 1 μM GSK2578215A, and 200 nM CZC25146 (kindly provided by Sabine Hilfiker but commercially available through Tocris and Sigma) was added at the 2-week time point and freshly supplemented every feeding for a total of 2 weeks. DMSO (1 μM and 200 nM) was used as the vehicle control.

Calcium Imaging

iPSC-derived sensory neuron cultures were functionally tested using ratiometric live-cell calcium imaging using dual-wavelength fluorescent calcium indicator FURA-2AM (Life Technologies) to detect intracellular calcium levels as described previously (Schwab and Ebert, 2014). Metafluor imaging software was used to detect and analyze intracellular calcium changes throughout the experiment (Molecular Devices), where a $\geq$20% increase in intracellular calcium from baseline constituted a response.

Western Blot

Whole-cell lysates were isolated from sensory neuron cultures using 1× Chaps Cell Extract buffer with protease inhibitors (Cell Signaling Technology). Twenty micrograms of protein was run on 10% Tris-HCl polyacrylamide gels (Bio-Rad), transferred to PVDF membrane (Millipore), and probed following standard methods. Primary antibodies used were rabbit anti-GAPDH (Sigma-Aldrich; G9545), rabbit anti-LRRK2 phospho S935 (Abcam; ab133450), rabbit anti-LRRK2 (Cell Signal; 5559), rabbit anti p62 (Novus; NBP1-48320), rabbit anti-LC3B (Cell Signal; 3868), mouse anti PHF-Tau (Thermo; MN1020), mouse anti-Tau (Cell Signal; 4019), and mouse anti-SNCA (DSHB; H3C-s). Secondary antibodies anti-rabbit IgG HRP (Promega; W4011) and anti-mouse IgG HRP (Promega; W4021) were used.

Immunocytochemistry

Plated cells were fixed in 4% paraformaldehyde in PBS (pH 7.4) for 20 min at room temperature. Nonspecific labeling was blocked and the cells permeabilized prior to primary antibody incubation. Cells were subsequently labeled with the appropriate fluorescently tagged secondary antibodies. Hoechst nuclear dye was used to label nuclei. Primary antibodies used were rabbit anti-peripherin (Millipore; AB1530), mouse anti-βIII tubulin (Promega; G7121), rabbit anti-TRPV1 (Novus Biologicals; NBP1-97417), mouse anti-tau (Cell Signal; 4019), rabbit anti-MAP2 (Cell Signal; 4542), rabbit anti-tyrosine hydroxylase (Pel-Freez; P40101-150), mouse anti-SNCA (DSHB; H3C-s), mouse anti-SNCA 211 (Thermo;

MA5-12272), mouse anti-ubiquitin (Novus Biologicals; NB300-130SS), mouse anti-LRRK2 (NeuroMab; clone N241A/34; 73-253), rabbit anti-LRRK2 phospho S935 (Abcam; ab133450), mouse anti-phospho-PHF-tau pSer202+Thr205 (Thermo Scientific; AT8; MN1020), and rabbit anti-ATF3 (Santa Cruz Biotechnology; C-19; sc-188). Secondary antibodies included donkey anti-mouse AF488 (Invitrogen; A21202) and goat anti-rabbit RhoRed (Invitrogen; R6394).

Imaging and Data Analysis

Data for each iPSC line are from two to six independent experiments with three technical replicates within each experiment. Within each immunocytochemistry-based experiment, at least five images were taken on each of at least three different fluorescently labeled coverslips per time point per line using a Nikon inverted microscope and Spot imaging software. The images were analyzed for antigen specificity using MetaMorph Software (Molecular Devices). Calcium imaging data were collected from a minimum of three coverslips per time point from each line. A minimum of 25 neurons were recorded from each coverslip. In all experiments, the evaluator was blinded to the cell line and treatment condition. Data were statistically analyzed with Prism software (GraphPad) first for normality using the D'Agostino-Pearson omnibus normality test, followed by the parametric one-way ANOVA and Tukey's multiple comparison test of significance or the non-parametric Kruskal-Wallis test and Dunn's multiple comparison test of significance; $\alpha = 0.05$. Student's t test was used when appropriate. Data are presented as the average ± SEM with the statistical test used indicated in each figure legend.

SUPPLEMENTAL INFORMATION

Supplemental Information includes Supplemental Experimental Procedures and five figures and can be found with this article online at http://dx.doi.org/10.1016/j.stemcr.2015.11.004.

ACKNOWLEDGMENTS

The authors thank S. Hilfiker (Spanish National Research Council) for providing kinase inhibitors and T. Patitucci (Medical College of Wisconsin) for critically reading the manuscript. The SNCA HC3 antibody was obtained from the Developmental Studies Hybridoma Bank at the University of Iowa. This work was funded in part through generous donations to the Medical College of Wisconsin for Parkinson's disease research and by a grant from Advancing a Healthier Wisconsin.

Received: July 1, 2015
Revised: November 11, 2015
Accepted: November 12, 2015
Published: December 8, 2015

REFERENCES

Alcalay, R.N., Mirelman, A., Saunders-Pullman, R., Tang, M.X., Mejia Santana, H., Raymond, D., Roos, E., Orbe-Reilly, M., Gurevich, T., Bar Shira, A., et al. (2013). Parkinson disease phenotype in Ashkenazi Jews with and without LRRK2 G2019S mutations. Mov. Disord. *28*, 1966–1971.

Alim, M.A., Hossain, M.S., Arima, K., Takeda, K., Izumiyama, Y., Nakamura, M., Kaji, H., Shinoda, T., Hisanaga, S., and Ueda, K. (2002). Tubulin seeds alpha-synuclein fibril formation. J. Biol. Chem. *277*, 2112–2117.

Anand, V.S., Reichling, L.J., Lipinski, K., Stochaj, W., Duan, W., Kelleher, K., Pungaliya, P., Brown, E.L., Reinhart, P.H., Somberg, R., et al. (2009). Investigation of leucine-rich repeat kinase 2 : enzymological properties and novel assays. FEBS J. *276*, 466–478.

Beach, T.G., Adler, C.H., Sue, L.I., Vedders, L., Lue, L., White Iii, C.L., Akiyama, H., Caviness, J.N., Shill, H.A., Sabbagh, M.N., and Walker, D.G.; Arizona Parkinson's Disease Consortium (2010). Multi-organ distribution of phosphorylated alpha-synuclein histopathology in subjects with Lewy body disorders. Acta Neuropathol. *119*, 689–702.

Biosa, A., Trancikova, A., Civiero, L., Glauser, L., Bubacco, L., Greggio, E., and Moore, D.J. (2013). GTPase activity regulates kinase activity and cellular phenotypes of Parkinson's disease-associated LRRK2. Hum. Mol. Genet. *22*, 1140–1156.

Boulting, G.L., Kiskinis, E., Croft, G.F., Amoroso, M.W., Oakley, D.H., Wainger, B.J., Williams, D.J., Kahler, D.J., Yamaki, M., Davidow, L., et al. (2011). A functionally characterized test set of human induced pluripotent stem cells. Nat. Biotechnol. *29*, 279–286.

Cartelli, D., Goldwurm, S., Casagrande, F., Pezzoli, G., and Cappelletti, G. (2012). Microtubule destabilization is shared by genetic and idiopathic Parkinson's disease patient fibroblasts. PLoS ONE *7*, e37467.

Cersosimo, M.G., and Benarroch, E.E. (2012). Pathological correlates of gastrointestinal dysfunction in Parkinson's disease. Neurobiol. Dis. *46*, 559–564.

Chambers, S.M., Qi, Y., Mica, Y., Lee, G., Zhang, X.J., Niu, L., Bilsland, J., Cao, L., Stevens, E., Whiting, P., et al. (2012). Combined small-molecule inhibition accelerates developmental timing and converts human pluripotent stem cells into nociceptors. Nat. Biotechnol. *30*, 715–720.

Cherra, S.J., 3rd, Steer, E., Gusdon, A.M., Kiselyov, K., and Chu, C.T. (2013). Mutant LRRK2 elicits calcium imbalance and depletion of dendritic mitochondria in neurons. Am. J. Pathol. *182*, 474–484.

Cookson, M.R., Hardy, J., and Lewis, P.A. (2008). Genetic neuropathology of Parkinson's disease. Int. J. Clin. Exp. Pathol. *1*, 217–231.

Cooper, O., Seo, H., Andrabi, S., Guardia-Laguarta, C., Graziotto, J., Sundberg, M., McLean, J.R., Carrillo-Reid, L., Xie, Z., Osborn, T., et al. (2012). Pharmacological rescue of mitochondrial deficits in iPSC-derived neural cells from patients with familial Parkinson's disease. Sci. Transl. Med. *4*, 141ra90.

Covy, J.P., and Giasson, B.I. (2009). Identification of compounds that inhibit the kinase activity of leucine-rich repeat kinase 2. Biochem. Biophys. Res. Commun. *378*, 473–477.

D'Andrea, M.R., Ilyin, S., and Plata-Salaman, C.R. (2001). Abnormal patterns of microtubule-associated protein-2 (MAP-2) immunolabeling in neuronal nuclei and Lewy bodies in Parkinson's disease substantia nigra brain tissues. Neurosci. Lett. *306*, 137–140.

Dabby, R., Djaldetti, R., Shahmurov, M., Treves, T.A., Gabai, B., Melamed, E., Sadeh, M., and Avinoach, I. (2006). Skin biopsy for assessment of autonomic denervation in Parkinson's disease. J Neural Transm (Vienna) *113*, 1169–1176.

Deng, X., Dzamko, N., Prescott, A., Davies, P., Liu, Q., Yang, Q., Lee, J.D., Patricelli, M.P., Nomanbhoy, T.K., Alessi, D.R., and Gray, N.S. (2011). Characterization of a selective inhibitor of the Parkinson's disease kinase LRRK2. Nat. Chem. Biol. *7*, 203–205.

Donadio, V., Incensi, A., Leta, V., Giannoccaro, M.P., Scaglione, C., Martinelli, P., Capellari, S., Avoni, P., Baruzzi, A., and Liguori, R. (2014). Skin nerve α-synuclein deposits: a biomarker for idiopathic Parkinson disease. Neurology *82*, 1362–1369.

Doppler, K., Ebert, S., Uçeyler, N., Trenkwalder, C., Ebentheuer, J., Volkmann, J., and Sommer, C. (2014). Cutaneous neuropathy in Parkinson's disease: a window into brain pathology. Acta Neuropathol. *128*, 99–109.

Dzamko, N., Deak, M., Hentati, F., Reith, A.D., Prescott, A.R., Alessi, D.R., and Nichols, R.J. (2010). Inhibition of LRRK2 kinase activity leads to dephosphorylation of Ser(910)/Ser(935), disruption of 14-3-3 binding and altered cytoplasmic localization. Biochem. J. *430*, 405–413.

Ebert, A.D., Yu, J., Rose, F.F., Jr., Mattis, V.B., Lorson, C.L., Thomson, J.A., and Svendsen, C.N. (2009). Induced pluripotent stem cells from a spinal muscular atrophy patient. Nature *457*, 277–280.

Ebert, A.D., Shelley, B.C., Hurley, A.M., Onorati, M., Castiglioni, V., Patitucci, T.N., Svendsen, S.P., Mattis, V.B., McGivern, J.V., Schwab, A.J., et al. (2013). EZ spheres: a stable and expandable culture system for the generation of pre-rosette multipotent stem cells from human ESCs and iPSCs. Stem Cell Res. (Amst.) *10*, 417–427.

Edwards, T.L., Scott, W.K., Almonte, C., Burt, A., Powell, E.H., Beecham, G.W., Wang, L., Züchner, S., Konidari, I., Wang, G., et al. (2010). Genome-wide association study confirms SNPs in SNCA and the MAPT region as common risk factors for Parkinson disease. Ann. Hum. Genet. *74*, 97–109.

Gaig, C., Vilas, D., Infante, J., Sierra, M., García-Gorostiaga, I., Buongiorno, M., Ezquerra, M., Martí, M.J., Valldeoriola, F., Aguilar, M., et al. (2014). Nonmotor symptoms in LRRK2 G2019S associated Parkinson's disease. PLoS ONE *9*, e108982.

Gatto, E.M., Parisi, V., Converso, D.P., Poderoso, J.J., Carreras, M.C., Martí-Massó, J.F., and Paisán-Ruiz, C. (2013). The LRRK2 G2019S mutation in a series of Argentinean patients with Parkinson's disease: clinical and demographic characteristics. Neurosci. Lett. *537*, 1–5.

Giasson, B.I., and Van Deerlin, V.M. (2008). Mutations in LRRK2 as a cause of Parkinson's disease. Neurosignals *16*, 99–105.

Gillardon, F. (2009). Leucine-rich repeat kinase 2 phosphorylates brain tubulin-beta isoforms and modulates microtubule stability–a point of convergence in parkinsonian neurodegeneration? J. Neurochem. *110*, 1514–1522.

Gómez-Suaga, P., Luzón-Toro, B., Churamani, D., Zhang, L., Bloor-Young, D., Patel, S., Woodman, P.G., Churchill, G.C., and Hilfiker, S. (2012). Leucine-rich repeat kinase 2 regulates autophagy through a calcium-dependent pathway involving NAADP. Hum. Mol. Genet. *21*, 511–525.

Greggio, E., Jain, S., Kingsbury, A., Bandopadhyay, R., Lewis, P., Kaganovich, A., van der Brug, M.P., Beilina, A., Blackinton, J., Thomas, K.J., et al. (2006). Kinase activity is required for the toxic effects of mutant LRRK2/dardarin. Neurobiol. Dis. *23*, 329–341.

Hasegawa, K., Stoessl, A.J., Yokoyama, T., Kowa, H., Wszolek, Z.K., and Yagishita, S. (2009). Familial parkinsonism: study of original Sagamihara PARK8 (I2020T) kindred with variable clinicopathologic outcomes. Parkinsonism Relat. Disord. *15*, 300–306.

HD iPSC Consortium (2012). Induced pluripotent stem cells from patients with Huntington's disease show CAG-repeat-expansion-associated phenotypes. Cell Stem Cell *11*, 264–278.

Hu, B.Y., Weick, J.P., Yu, J., Ma, L.X., Zhang, X.Q., Thomson, J.A., and Zhang, S.C. (2010). Neural differentiation of human induced pluripotent stem cells follows developmental principles but with variable potency. Proc. Natl. Acad. Sci. USA *107*, 4335–4340.

Ikemura, M., Saito, Y., Sengoku, R., Sakiyama, Y., Hatsuta, H., Kanemaru, K., Sawabe, M., Arai, T., Ito, G., Iwatsubo, T., et al. (2008). Lewy body pathology involves cutaneous nerves. J. Neuropathol. Exp. Neurol. *67*, 945–953.

Jaleel, M., Nichols, R.J., Deak, M., Campbell, D.G., Gillardon, F., Knebel, A., and Alessi, D.R. (2007). LRRK2 phosphorylates moesin at threonine-558: characterization of how Parkinson's disease mutants affect kinase activity. Biochem. J. *405*, 307–317.

Kawakami, F., Yabata, T., Ohta, E., Maekawa, T., Shimada, N., Suzuki, M., Maruyama, H., Ichikawa, T., and Obata, F. (2012). LRRK2 phosphorylates tubulin-associated tau but not the free molecule: LRRK2-mediated regulation of the tau-tubulin association and neurite outgrowth. PLoS ONE *7*, e30834.

Kett, L.R., Boassa, D., Ho, C.C., Rideout, H.J., Hu, J., Terada, M., Ellisman, M., and Dauer, W.T. (2012). LRRK2 Parkinson disease mutations enhance its microtubule association. Hum. Mol. Genet. *21*, 890–899.

Law, B.M., Spain, V.A., Leinster, V.H., Chia, R., Beilina, A., Cho, H.J., Taymans, J.M., Urban, M.K., Sancho, R.M., Blanca Ramírez, M., et al. (2014). A direct interaction between leucine-rich repeat kinase 2 and specific β-tubulin isoforms regulates tubulin acetylation. J. Biol. Chem. *289*, 895–908.

Lee, B.D., Shin, J.H., VanKampen, J., Petrucelli, L., West, A.B., Ko, H.S., Lee, Y.I., Maguire-Zeiss, K.A., Bowers, W.J., Federoff, H.J., et al. (2010). Inhibitors of leucine-rich repeat kinase-2 protect against models of Parkinson's disease. Nat. Med. *16*, 998–1000.

Li, Y., Dunn, L., Greggio, E., Krumm, B., Jackson, G.S., Cookson, M.R., Lewis, P.A., and Deng, J. (2009a). The R1441C mutation alters the folding properties of the ROC domain of LRRK2. Biochim. Biophys. Acta *1792*, 1194–1197.

Li, Y., Liu, W., Oo, T.F., Wang, L., Tang, Y., Jackson-Lewis, V., Zhou, C., Geghman, K., Bogdanov, M., Przedborski, S., et al. (2009b). Mutant LRRK2(R1441G) BAC transgenic mice recapitulate cardinal features of Parkinson's disease. Nat. Neurosci. *12*, 826–828.

Lin, C.H., Tsai, P.I., Wu, R.M., and Chien, C.T. (2010). LRRK2 G2019S mutation induces dendrite degeneration through mislocalization and phosphorylation of tau by recruiting autoactivated GSK3ß. J. Neurosci. *30*, 13138–13149.

Lindå, H., Sköld, M.K., and Ochsmann, T. (2011). Activating transcription factor 3, a useful marker for regenerative response after nerve root injury. Front. Neurol. *2*, 30.

Lindwall, G., and Cole, R.D. (1984). Phosphorylation affects the ability of tau protein to promote microtubule assembly. J. Biol. Chem. *259*, 5301–5305.

Luerman, G.C., Nguyen, C., Samaroo, H., Loos, P., Xi, H., Hurtado-Lorenzo, A., Needle, E., Stephen Noell, G., Galatsis, P., Dunlop, J., et al. (2014). Phosphoproteomic evaluation of pharmacological inhibition of leucine-rich repeat kinase 2 reveals significant off-target effects of LRRK-2-IN-1. J. Neurochem. *128*, 561–576.

Luzón-Toro, B., Rubio de la Torre, E., Delgado, A., Pérez-Tur, J., and Hilfiker, S. (2007). Mechanistic insight into the dominant mode of the Parkinson's disease-associated G2019S LRRK2 mutation. Hum. Mol. Genet. *16*, 2031–2039.

MacLeod, D., Dowman, J., Hammond, R., Leete, T., Inoue, K., and Abeliovich, A. (2006). The familial Parkinsonism gene LRRK2 regulates neurite process morphology. Neuron *52*, 587–593.

Marras, C., Schüle, B., Munhoz, R.P., Rogaeva, E., Langston, J.W., Kasten, M., Meaney, C., Klein, C., Wadia, P.M., Lim, S.Y., et al. (2011). Phenotype in parkinsonian and nonparkinsonian LRRK2 G2019S mutation carriers. Neurology *77*, 325–333.

Melrose, H.L., Kent, C.B., Taylor, J.P., Dachsel, J.C., Hinkle, K.M., Lincoln, S.J., Mok, S.S., Culvenor, J.G., Masters, C.L., Tyndall, G.M., et al. (2007). A comparative analysis of leucine-rich repeat kinase 2 (Lrrk2) expression in mouse brain and Lewy body disease. Neuroscience *147*, 1047–1058.

Melrose, H.L., Dächsel, J.C., Behrouz, B., Lincoln, S.J., Yue, M., Hinkle, K.M., Kent, C.B., Korvatska, E., Taylor, J.P., Witten, L., et al. (2010). Impaired dopaminergic neurotransmission and microtubule-associated protein tau alterations in human LRRK2 transgenic mice. Neurobiol. Dis. *40*, 503–517.

Mu, L., Sobotka, S., Chen, J., Su, H., Sanders, I., Adler, C.H., Shill, H.A., Caviness, J.N., Samanta, J.E., and Beach, T.G.; Arizona Parkinson's Disease Consortium (2013a). Alpha-synuclein pathology and axonal degeneration of the peripheral motor nerves innervating pharyngeal muscles in Parkinson disease. J. Neuropathol. Exp. Neurol. *72*, 119–129.

Mu, L., Sobotka, S., Chen, J., Su, H., Sanders, I., Nyirenda, T., Adler, C.H., Shill, H.A., Caviness, J.N., Samanta, J.E., et al.; Arizona Parkinson's Disease Consortium (2013b). Parkinson disease affects peripheral sensory nerves in the pharynx. J. Neuropathol. Exp. Neurol. *72*, 614–623.

Nolano, M., Provitera, V., Estraneo, A., Selim, M.M., Caporaso, G., Stancanelli, A., Saltalamacchia, A.M., Lanzillo, B., and Santoro, L. (2008). Sensory deficit in Parkinson's disease: evidence of a cutaneous denervation. Brain *131*, 1903–1911.

Ohta, E., Nihira, T., Uchino, A., Imaizumi, Y., Okada, Y., Akamatsu, W., Takahashi, K., Hayakawa, H., Nagai, M., Ohyama, M., et al. (2015). I2020T mutant LRRK2 iPSC-derived neurons in the Sagamihara family exhibit increased Tau phosphorylation through the AKT/GSK-3β signaling pathway. Hum. Mol. Genet. *24*, 4879–4900.

Orimo, S., Uchihara, T., Nakamura, A., Mori, F., Kakita, A., Wakabayashi, K., and Takahashi, H. (2008). Axonal alpha-synuclein aggregates herald centripetal degeneration of cardiac sympathetic nerve in Parkinson's disease. Brain *131*, 642–650.

Parisiadou, L., Xie, C., Cho, H.J., Lin, X., Gu, X.L., Long, C.X., Lobbestael, E., Baekelandt, V., Taymans, J.M., Sun, L., and Cai, H. (2009). Phosphorylation of ezrin/radixin/moesin proteins by LRRK2 promotes the rearrangement of actin cytoskeleton in neuronal morphogenesis. J. Neurosci. *29*, 13971–13980.

Pont-Sunyer, C., Hotter, A., Gaig, C., Seppi, K., Compta, Y., Katzenschlager, R., Mas, N., Hofeneder, D., Brücke, T., Bayés, A., et al. (2015). The onset of nonmotor symptoms in Parkinson's disease (the ONSET PD study). Mov. Disord. *30*, 229–237.

Ramonet, D., Daher, J.P., Lin, B.M., Stafa, K., Kim, J., Banerjee, R., Westerlund, M., Pletnikova, O., Glauser, L., Yang, L., et al. (2011). Dopaminergic neuronal loss, reduced neurite complexity and autophagic abnormalities in transgenic mice expressing G2019S mutant LRRK2. PLoS ONE *6*, e18568.

Reinhardt, P., Schmid, B., Burbulla, L.F., Schöndorf, D.C., Wagner, L., Glatza, M., Höing, S., Hargus, G., Heck, S.A., Dhingra, A., et al. (2013). Genetic correction of a LRRK2 mutation in human iPSCs links parkinsonian neurodegeneration to ERK-dependent changes in gene expression. Cell Stem Cell *12*, 354–367.

Reith, A.D., Bamborough, P., Jandu, K., Andreotti, D., Mensah, L., Dossang, P., Choi, H.G., Deng, X., Zhang, J., Alessi, D.R., and Gray, N.S. (2012). GSK2578215A; a potent and highly selective 2-arylmethyloxy-5-substitutent-N-arylbenzamide LRRK2 kinase inhibitor. Bioorg. Med. Chem. Lett. *22*, 5625–5629.

Sánchez-Danés, A., Richaud-Patin, Y., Carballo-Carbajal, I., Jiménez-Delgado, S., Caig, C., Mora, S., Di Guglielmo, C., Ezquerra, M., Patel, B., Giralt, A., et al. (2012). Disease-specific phenotypes in dopamine neurons from human iPS-based models of genetic and sporadic Parkinson's disease. EMBO Mol. Med. *4*, 380–395.

Schwab, A.J., and Ebert, A.D. (2014). Sensory neurons do not induce motor neuron loss in a human stem cell model of spinal muscular atrophy. PLoS ONE *9*, e103112.

Shanley, M.R., Hawley, D., Leung, S., Zaidi, N.F., Dave, R., Schlosser, K.A., Bandopadhyay, R., Gerber, S.A., and Liu, M. (2015). LRRK2 Facilitates tau Phosphorylation through Strong Interaction with tau and cdk5. Biochemistry *54*, 5198–5208.

Shishido, T., Ikemura, M., Obi, T., Yamazaki, K., Terada, T., Sugiura, A., Saito, Y., Murayama, S., and Mizoguchi, K. (2010). alpha-synuclein accumulation in skin nerve fibers revealed by skin biopsy in pure autonomic failure. Neurology *74*, 608–610.

Si-Tayeb, K., Noto, F.K., Sepac, A., Sedlic, F., Bosnjak, Z.J., Lough, J.W., and Duncan, S.A. (2010). Generation of human induced pluripotent stem cells by simple transient transfection of plasmid DNA encoding reprogramming factors. BMC Dev. Biol. *10*, 81.

Simón-Sánchez, J., Schulte, C., Bras, J.M., Sharma, M., Gibbs, J.R., Berg, D., Paisan-Ruiz, C., Lichtner, P., Scholz, S.W., Hernandez, D.G., et al. (2009). Genome-wide association study reveals genetic risk underlying Parkinson's disease. Nat. Genet. *41*, 1308–1312.

Smith, W.W., Pei, Z., Jiang, H., Dawson, V.L., Dawson, T.M., and Ross, C.A. (2006). Kinase activity of mutant LRRK2 mediates neuronal toxicity. Nat. Neurosci. *9*, 1231–1233.

Taymans, J.M., and Cookson, M.R. (2010). Mechanisms in dominant parkinsonism: The toxic triangle of LRRK2, alpha-synuclein, and tau. BioEssays *32*, 227–235.

Toth, C., Breithaupt, K., Ge, S., Duan, Y., Terris, J.M., Thiessen, A., Wiebe, S., Zochodne, D.W., and Suchowersky, O. (2010). Levodopa, methylmalonic acid, and neuropathy in idiopathic Parkinson disease. Ann. Neurol. *68*, 28–36.

Toulouse, A., and Sullivan, A.M. (2008). Progress in Parkinson's disease-where do we stand? Prog. Neurobiol. *85*, 376–392.

Trinh, J., Amouri, R., Duda, J.E., Morley, J.F., Read, M., Donald, A., Vilariño-Güell, C., Thompson, C., Szu Tu, C., Gustavsson, E.K., et al. (2014). Comparative study of Parkinson's disease and leucine-rich repeat kinase 2 p.G2019S parkinsonism. Neurobiol. Aging *35*, 1125–1131.

Tsika, E., Nguyen, A.P., Dusonchet, J., Colin, P., Schneider, B.L., and Moore, D.J. (2015). Adenoviral-mediated expression of G2019S LRRK2 induces striatal pathology in a kinase-dependent manner in a rat model of Parkinson's disease. Neurobiol. Dis. *77*, 49–61.

Tsujino, H., Kondo, E., Fukuoka, T., Dai, Y., Tokunaga, A., Miki, K., Yonenobu, K., Ochi, T., and Noguchi, K. (2000). Activating transcription factor 3 (ATF3) induction by axotomy in sensory and motoneurons: A novel neuronal marker of nerve injury. Mol. Cell. Neurosci. *15*, 170–182.

Tysnes, O.B., Müller, B., and Larsen, J.P. (2010). Are dysautonomic and sensory symptoms present in early Parkinson's disease? Acta Neurol. Scand. Suppl. (190), 72–77.

van der Heeden, J.F., Marinus, J., Martinez-Martin, P., and van Hilten, J.J. (2014). Importance of nondopaminergic features in evaluating disease severity of Parkinson disease. Neurology *82*, 412–418.

Wakabayashi, K., and Takahashi, H. (1997). Neuropathology of autonomic nervous system in Parkinson's disease. Eur. Neurol. *38* (*Suppl 2*), 2–7.

Waxman, E.A., Covy, J.P., Bukh, I., Li, X., Dawson, T.M., and Giasson, B.I. (2009). Leucine-rich repeat kinase 2 expression leads to aggresome formation that is not associated with alpha-synuclein inclusions. J. Neuropathol. Exp. Neurol. *68*, 785–796.

West, A.B., Moore, D.J., Biskup, S., Bugayenko, A., Smith, W.W., Ross, C.A., Dawson, V.L., and Dawson, T.M. (2005). Parkinson's disease-associated mutations in leucine-rich repeat kinase 2 augment kinase activity. Proc. Natl. Acad. Sci. USA *102*, 16842–16847.

Xiao, S., McLean, J., and Robertson, J. (2006). Neuronal intermediate filaments and ALS: a new look at an old question. Biochim. Biophys. Acta *1762*, 1001–1012.

Yang, F., Jiang, Q., Zhao, J., Ren, Y., Sutton, M.D., and Feng, J. (2005). Parkin stabilizes microtubules through strong binding mediated by three independent domains. J. Biol. Chem. *280*, 17154–17162.

Zhu, X., Siedlak, S.L., Smith, M.A., Perry, G., and Chen, S.G. (2006). LRRK2 protein is a component of Lewy bodies. Ann. Neurol. *60*, 617–618, author reply 618–619.